Applied and Computational Mechanics 4 (2010) 191–200

Ductile-brittle behavior at blunted cavities in 3D iron crystals uncovered and covered by copper atoms

V. Pelikán[a,*], P. Hora[a], O. Červená[a], A. Spielmannová[b], A. Machová[b]

[a] *Institute of Thermomechanics of the ASCR, v.v.i., Veleslavínova 11, 301 14 Plzeň, Czech Republic*
[b] *Institute of Thermomechanics of the ASCR, v.v.i., Dolejškova 5, 182 00 Praha, Czech Republic*

Received 27 August 2009; received in revised form 12 November 2010

Abstract

This paper is devoted to studies of the mechanical response of an atomically blunted cavity uncovered and covered by copper atoms by means 3D molecular dynamic (MD) simulations. The cavity is loaded uni-axially in tension mode I. Our question is how the copper atoms influence the ductile-brittle behavior at the crack front of the blunted cavity in comparison with the blunted cavity in pure bcc iron. We show that the dislocation emission is easier in the Fe–Cu system in comparison with pure bcc iron. However, stability of the blunted cavities seems to be weaker in copper region than in pure bcc iron.

Keywords: molecular dynamics, bcc iron crystal, blunted cavity, copper cover, ductile-brittle behavior

1. Introduction

Molecular dynamic (MD) simulation is a valuable tool in material science since it provides information on the micromechanics and kinetics of failure in materials, which is often not accessible from experiments. Much attention has been devoted to bcc (body centered cubic) iron and Fe–Cu system, both in experiments (see e.g. [9, 15, 16, 17, 19]) and theoretical studies [1, 8, 10, 11, 13, 14, 18] because of their importance in structural steel applications, including older reactor ferritic steels. While older experimental observations in the model Fe–Cu dilute alloys brought information concerning bcc Cu nano-particles [17, 19], recent experimental findings show [15] that vacancy-Cu complexes formed by irradiation aggregate into nano-voids where inner surface of the nano–voids is covered by Cu atoms.

Unlike our previous 3D crack simulations [7, 14, 18] where narrow cracks in bcc iron and in Fe–Cu system were studied by means of MD simulations, this paper is devoted to studies of the mechanical response of an atomically blunted cavity uncovered and covered by copper atoms, which was observed in mentioned experiments [15]. Our question is how the copper atoms influence the ductile-brittle behavior at the crack front in comparison with pure bcc iron.

The paper shows that the dislocation emission is easier in the Fe–Cu system in comparison with pure bcc iron. However, stability of the blunted cavities seems to be weaker in copper region than in pure bcc iron.

*Corresponding author. Tel.: +420 377 236 415, e-mail: pelikan@cdm.it.cas.cz.

2. MD simulations

Similar to [18], the bcc iron crystal has basic cubic orientation $\{100\}$ and we use our MD code for parallel processing with Message Passing Interface. Interatomic interactions in bcc iron and in Fe–Cu system are described using semi-empirical many-body potentials presented in [1] that are based on tight binding model from quantum mechanics. We consider a pre-existing central Griffith (through) cavity loaded in tension mode I. The cavity was introduced by removing part of atoms in 3 planes, so its initial blunting corresponds to 2 a_0, where $a_0 = 2.866\,5$ Å is the lattice parameter of bcc iron. The cavity is relatively long, its half crack length is $l_0 = 100a_0$. The crystal consist of 1999 planes in the $x = [100]$ direction of the potential crack extension (width W), 99 planes along the crack front in the $y = [010]$ direction (thickness B) and 1999 planes in the $z = [001]$ direction (length L) of loading. The crystal contains about 100 million of atoms (more precisely, the number of atoms is $N = 98\,921\,249$). Since the interatomic potentials are short ranged, the cavity surfaces perpendicular to z-axis are free of forces. While inside the perfect unloaded lattice the resulting forces at individual atoms are zero, there are unresolved forces at free surfaces of the sample due to missing interatomic bonds. Therefore, surface relaxation was performed before loading to avoid its influence on crack tip processes.

Copper atoms are initially set on bcc iron lattice. It recalls internal stress in copper region since the lattice parameter in bcc copper is larger [1] than in bcc iron. The relaxation mentioned above decreases also the internal stress in copper region, which was studied in detail for the basic cubic orientation in [13].

Newtonian equations of motion for the individual atoms have been solved by a central difference method using time integration step $h = 1 \times 10^{-14}$ s. The samples were loaded symmetrically in the $\langle 001 \rangle$ directions by prescribing external forces distributed homogeneously at individual atoms lying on the lower and upper surface layer. Each time step $t = nh$ we monitored the total number of existing interactions and global energy balance in the system. The crystal was loaded by external forces gradually (linearly), according to the scheme for 0 K in [18, fig. 2] with loading rate 0.014 GPa/ps. Initial atomic velocities in simulations were zero and the further thermal atomic motion was not controlled, i.e. during loading no atomic velocities are prescribed and our computer experiments after loading represent low temperature simulations with low total kinetic energy in the system.

Three different configurations were studied without any periodic boundary conditions:
i) the blunted cavity in pure bcc iron; ii) the blunted cavity covered by six copper layers; iii) the blunted cavity covered by two layers of copper atoms. These studies represent free 3D simulations.

In the fourth configuration, left corner of the cavity along the crack front was covered by a small Cu inclusion (of the area 8×8 atoms) and these simulations utilized a periodic boundary condition in the x-direction. Here, the total number of atoms is somewhat different, $N = 98\,921\,249$.

The crack tip processes in 3D are visualized along the crack front, i.e. in the atomic planes of the type (010), perpendicular to the crack front. It enabled 3D graphic output files representing a detail at the crack front with atomic coordinates, saved at prescribed time steps for further analysis. These files were relatively small due to a large memory and space requirements in further graphic treatments of the results. To recognize the slip patterns coming from the different slip planes, we also performed "block like shear" (BLS) simulations in 3D perfect bcc iron crystals.

3. Results and Discussions

We present results by means of details only at the left corner of the cavity since situation at the right corner is similar.

Each bond breakage or dislocation emission or etc. in the system leads to the stress relaxation at the crack front, which causes acoustic emission of the stress waves propagating in all directions toward free sample surfaces where the waves are reflected back to the interior of the crystal and may influence the situation at cavity region. Our 3D simulations after the first microscopic event are influenced soon by the back reflections due to small sample thickness B (after $90h$). As to lateral back reflections (along length L), the fastest longitudinal waves in the $\langle 001 \rangle$ directions ($C_L = 5\,550$ m/s) in our relatively large samples requires 5 164 time steps for the back stress wave reflections in the direction of loading, while 4648 time steps in the direction of potential crack extension (along width W). We are trying to present results that are not influenced by the lateral back wave reflections after dislocation emission or bond breakage at the crack front. Note that the back wave reflections influence the situation also in fracture experiments, but their influence is less intensive than in free 3D atomistic simulations. Here we are focused on comparison of 3D atomistic results in pure bcc iron and in Fe–Cu system. Since the atomistic samples have the same geometry in both cases, the most important influence on different behavior in the two systems plays the wave reflections from the Fe–Cu interfaces, which cannot be avoided, similar to scattering of the loading waves at the free cavity surfaces.

3.1. Blunted cavity in pure bcc iron

Fig. 1 shows the atomic configuration in the unloaded stage on two surface layers (distinguished by two different color atoms) where plane stress conditions must be fulfilled. In the middle of our thin crystal the stress state is neither plane strain nor plane stress but something between, with prevailing plane strain at the crack front. The Griffith stress needed for cleavage growth of our cavity corresponds to values $\sigma_G = 2.72$ GPa for plane strain and $\sigma_G = 2.64$ GPa for plane stress conditions, as follows from the analysis presented in [18]. The lower Griffith level is reached at the loaded borders at time step $18\,857h$ while at the plane placed in the middle of the crystal it is later due to flight time correction for the longitudinal loading waves, which

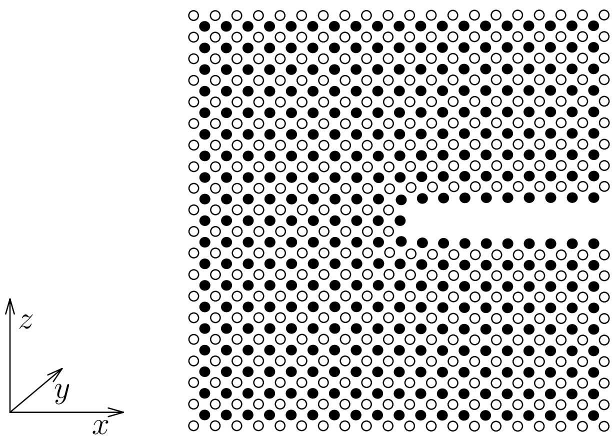

Fig. 1. Initial cavity blunting in pure bcc iron, a detail at left cavity corner

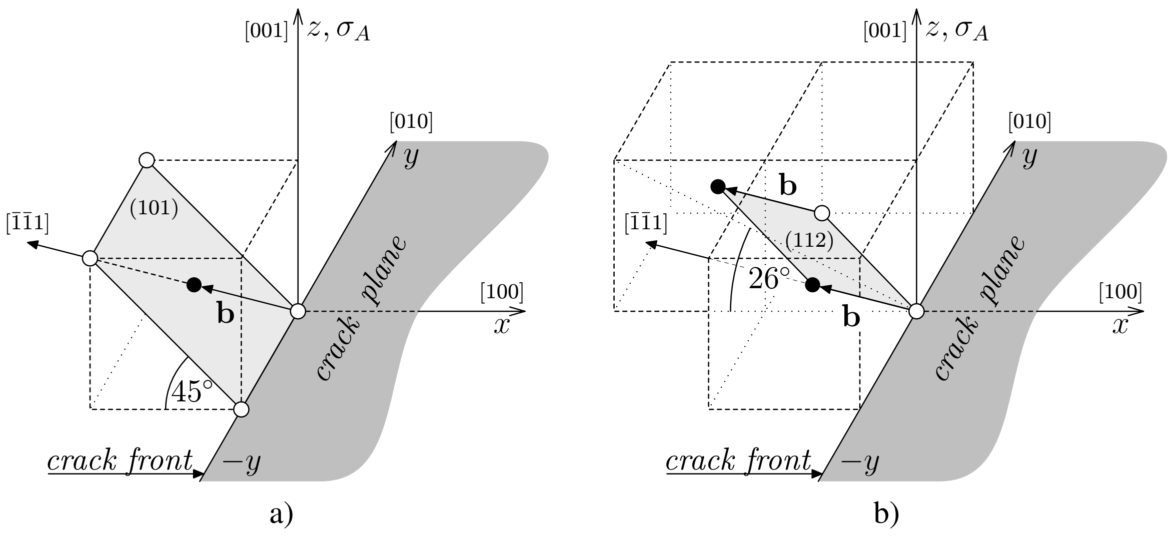

Fig. 2. Scheme of the inclined slip system $\langle 111\rangle\{101\}$ a) and $\langle 111\rangle\{112\}$ b) at the crack front

corresponds to $2\,582h$ [18]. It means that the critical stress concentration for cleavage in the middle of the crystal can be reached at time step by about $21\,439h$. Unlike [18], we did not observe brittle crack initiation in pure bcc iron in the present simulation with the atomically blunted cavity shown in fig. 1. It can be explained by the fact that a larger blunting decreases the stress concentration at the crack front. According to isotropic Goodier's continuum solution, presented e.g. in [4], it depends on the ratio of the initial half crack opening versus half crack length. This ratio in [18] corresponds to $c_0/l_0 = 1/200$, while here (see fig. 1) it is $c_0/l_0 = 1/100$. The larger blunting in the present paper decreases the concentration of the normal stress component at the crack front by a factor 2 according to Goodier's solution. More precise anisotropic solution by Savin [21] for our crystal orientation is presented in [22]. We observed the beginning of slip processes at time step 24 000 at the lower corner of our blunted cavity on free surface perpendicular to the crack front, which was identified as a dislocation emission on the inclined slip plane $\{101\}$ by means of BLS simulation mentioned above. This slip system is schematically shown in fig. 2a. It is visible that the $\langle 111\rangle\{101\}$ slip system is inclined at the angle $45°$ with respect to the $x = [100]$ direction. The second available but oblique slip system $\langle 111\rangle\{112\}$ is shown in fig. 2b. Note that the inclined slip systems contain the crack front, while the oblique slip systems intersect the crack front. As mentioned already in [18], these two slip systems have larger Schmid factor than the third possible slip system $\{123\}$ in bcc iron. Particularly in case of a perfect crystal with our orientation, the nominal shear stresses acting in the individual slip systems are:

$$\begin{aligned}\langle 111\rangle\{110\} &: \ \tau = 0.41\sigma_A,\\ \langle 111\rangle\{112\} &: \ \tau = 0.47\sigma_A,\\ \langle 111\rangle\{123\} &: \ \tau = 0.15\sigma_A.\end{aligned}$$

In comparison with a perfect crystal where validity of the Schmid law is expected, the presence of a crack or cavity causes stress intensification at the crack front (including the shear stress) as discussed in detail in [18]. The slip processes in [18] start by emission of dislocations in the $\langle 111\rangle\{101\}$ from the corner where the crack penetrates the free sample surfaces since the stress state here is more favorable than in the middle of the crystal [18]. It is in a qualitative agreement with the presented results. However, cross slip of the dislocations to $\langle 111\rangle\{112\}$

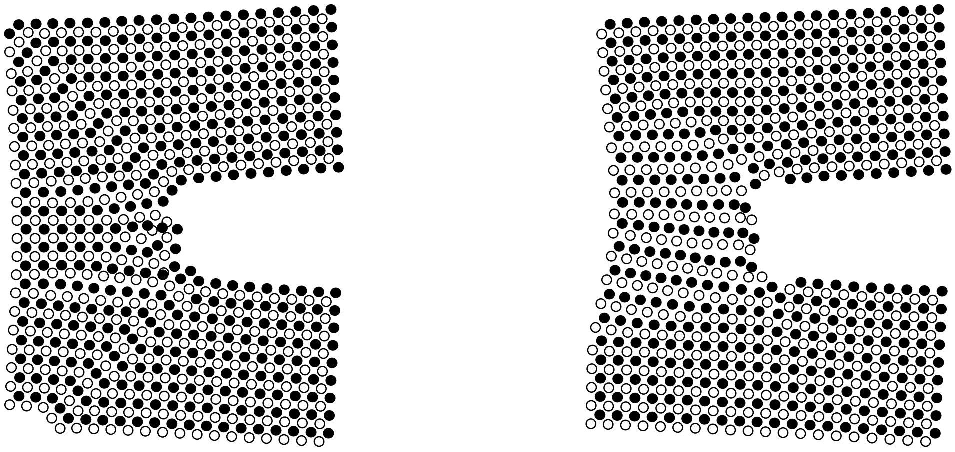

a) b)

Fig. 3. Detail of the atomic configuration at the left corner of the cavity in pure bcc iron at time step $24\,500h$; a) dislocation emission in the $\langle 111\rangle\{101\}$ inclined slip systems, the first two surface layers; b) situation in the layers 43–44 near the middle of the crystal

slip systems was monitored later in [18]. Here, until time step 25 000 when the simulation was terminated, the slip patterns from the $\langle 111\rangle\{112\}$ slip system at the blunted cavity were not observed. We observed only the patterns from the inclined slip systems $\langle 111\rangle\{101\}$ which illustrates fig. 3 at time step 24 500 where symmetric atomic configuration at the crystal surface (fig. 3a) and near the middle of the crystal (fig. 3b, layer 43–44) are shown under higher applied stress $\sigma_A = 3.429$ GPa. The slip patterns in fig. 3a containing three black and white atoms and starting from the cavity corners come from the double emission of dislocations on the $\langle 111\rangle\{101\}$ slip systems, which follows from BLS simulations. These patterns disappear in the middle of the crystal since the dislocations emitted from the free surface perpendicular to the crack front may finish at the free cavity surface along the crack front, similar to what is illustrated in [18, fig. 9]. While the cavity in fig. 3a is blunted and stable due to dislocation emission, certain structural changes in front of the cavity are visible in the middle of fig. 3b, leading to a possibility of small crack deflections at the corners after the plastic deformation described above. Such a small crack deflection is observed in the middle of the crystal. Dislocation emission on $\{101\}$ planes occurs first, since the stress barrier for dislocation generation on $\{101\}$ planes $\tau_c = 14.5$ GPa is smaller [18] than $\tau_c = 16.3$ GPa on $\{112\}$ slip planes. This barrier can still be decreased due to the presence of the so-called T-stress acting parallel to crack plane similar to stress component σ_{xx}. For a narrow cavity and our basic cubic orientation $T = Re(\mu_1\mu_2)\sigma_A$, where $Re(\mu_1\mu_2) \sim -1$ [22], similar to isotropic continuum. By Rice [20], it may decrease the stress barrier according to a simple interchange $\tau_c \to \tau_c + T\sin\theta\cos\theta$.

In our case, the angular function occurring in the later relation should be replaced by Schmid factor for the $\langle 111\rangle\{101\}$ slip system viewed in fig. 2a. It gives an estimate
$\langle 111\rangle\{101\}:\ \tau_c = 14.5\ \text{GPa} - 0.41\sigma_A$.

Note that the stress barriers given above correspond to a generation of straight edge dislocations in BLS simulations. In free 3D simulations, curved dislocations (see e.g. [18] or [7]) of mixed type (with screw and edge components) are emitted since they have lower net strain energy. It again decreases the stress barrier for dislocation generation in 3D.

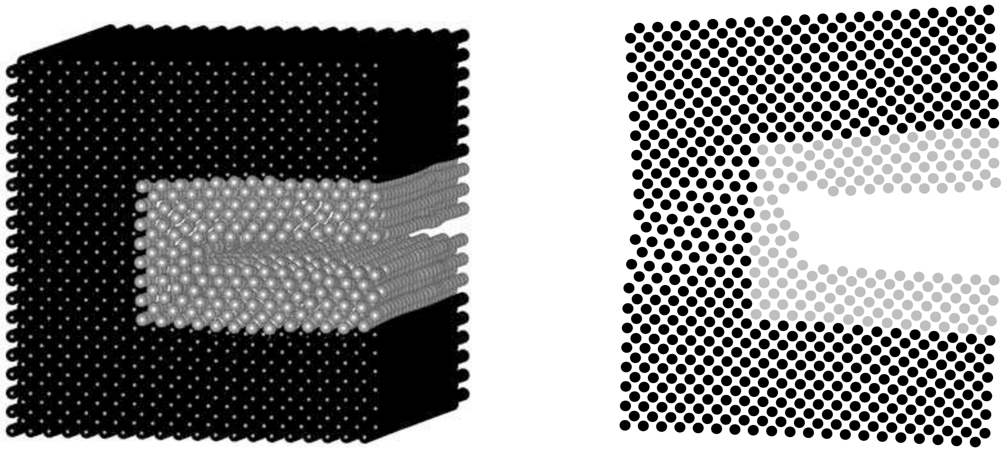

a) b)

Fig. 4. a) 3D-detail of the initial configuration at the left corner. b) Detail of atomic configuration in the middle of the crystal, time step $19\,200h$

In comparison with the results in [18] for 0 K and the narrow crack, in this study with the initially blunted cavity (fig. 1) under the same loading conditions, we detected the brittle→ductile transition caused by the initial blunting. The blunted cavity in fig. 3 is stable at the applied stress $\sigma_A \sim 1.3\,\sigma_G$, significantly above the Griffith level for plane stress. According to isotropic continuum predictions presented in [2, 5] this ductile behavior is theoretically possible in bcc iron at 0 K. The prediction in [5] is based on Peierls-Nabarro model and it depends on several dimensionless parameters e.g. $\gamma_{us}/2\gamma_s$, $\rho/c_0 = c_0/l_0$ and the angle θ . Here, $\gamma_{us} = 0.992\,4$ J/m^2 is the unstable stacking fault energy describing the energy barrier for dislocation generation in the slip system $\langle 111\rangle\{101\}$, $2\gamma_s = 3.624$ J/m^2 is the surface formation energy [12] needed for cleavage between the $\{001\}$ planes. The parameters $\gamma_{us}/2\gamma_s = 0.274$ and $\theta = 45°$ are the same for this study and the paper [18]. The parameter c_0/l_0 is different: in [18] it is $c_0/l_0 = 0.005$, here it is $c_0/l_0 = 0.01$. It lies close to the borders for the brittle→ductile transition predicted in [5, fig. 8]. The different (more simple) prediction [2] predicts brittle behavior at sharp cracks in bcc iron, while ductile behavior for significantly blunted cavities in bcc iron and so, the agreement or disagreement with the continuum isotropic predictions cannot be decided. More precise analysis requires include into continuum models [2, 5] the effects given by anisotropy, T-stress and normal relaxation in the slip system [3] (which is accessible only at UCSB).

3.2. Blunted cavity covered by a thick film of copper atoms

Detail from the initial 3D configuration at the left corner is shown in fig. 4a, where the iron atoms are shown by black color and copper atoms by gray color. After loading, a small crack deflection in the middle of the crystal occurred already at time step 19 200 (fig. 4b) when the applied stress corresponded to $\sigma_A = 2.687$ GPa, which is about $1.02\,\sigma_G$. It happened probably after an attempt to emit dislocation from the upper cavity surface into $\langle 111\rangle\{101\}$ slip systems, as the pairs of yellow and green copper atoms indicate at the upper corner. Dislocation emission in $\langle 111\rangle\{101\}$ slip systems started from free sample surface between time steps 19 600–19 700. In comparison with the cavity in pure bcc iron, the cavity covered a thick film of copper atoms is less stable. The reason of the asymmetry in fig. 4b is uncertain. It could be caused by the fact that the bcc copper with the used potential from [1] is metastable and dislocation generation

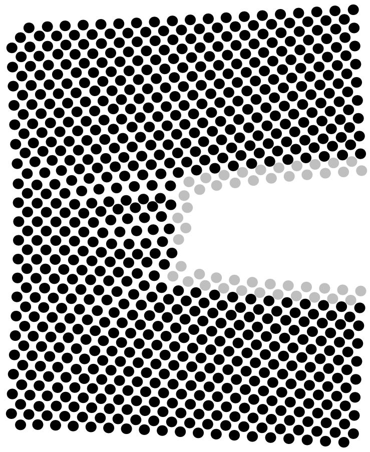

a)

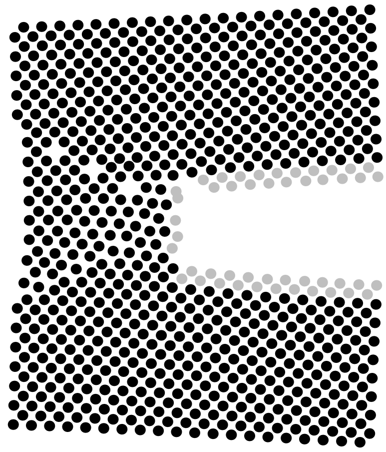

b)

Fig. 5. Dislocations at the left corner of the cavity covered by a thin film of copper atoms at time step $20\,900h$; a) symmetric dislocation emission in the inclined slip systems $\langle 111\rangle\{101\}$ on the first two surfaces layers; b) dislocations on the oblique slip planes 112 at the upper corner of the cavity in the middle of the crystal (layers 49–50)

may recall their structural instability, especially at a corner with higher stress concentration. It was observed also in 2D simulations presented in [19] and in 3D simulations [14] with different crack orientation. The second possibility for the asymmetry is different level of the residual stress at the corners after surface relaxation. Note that at time step 24 500 (comparable with pure bcc iron in fig. 3), the atomic structure in front of the crack front in this Fe–Cu system is more damaged and an asymmetric crack deflection is monitored. This situation can be already influenced by the back stress wave reflections and by absorption of the energy in the system via random thermal atomic motion, which is possible in nonlinear atomistic force models as in our case, unlike harmonic models with parabolic potentials that lead to linear force model and do not enable spontaneous thermal expansion and absorption in the atomic lattice.

3.3. Blunted cavity covered by a thin film of copper atoms

In this case the dislocation emission in the $\langle 111\rangle\{101\}$ inclined slip systems was monitored at the crystal surface already at time step 19 800, unlike pure bcc iron where no traces of dislocation emission were detected at the same time step. Detail from atomic configuration on the surface and in the middle of the crystal is shown in fig. 5a and fig. 5b at time step 20 900 when $\sigma_A = 2.925$ GPa which corresponds to about $1.1\ \sigma_G$. While on the crystal surface (fig. 5a) one may see symmetric slip patterns coming from dislocation emission in the $\langle 111\rangle\{101\}$ slip system, in the middle of the crystal at the upper corner one can see slip patterns (with empty atomic positions) coming from the slip of a dislocation on the oblique $\{112\}$ planes. Again, these patterns have been identified by means of BLS simulations in a small 3D iron crystal. As discussed in detail in [18], these patterns can arise after cross slip of screw dislocation from a $\{101\}$ plane to a $\{112\}$ plane (see [18, fig. 9]) or by direct dislocation emission from the crack front in the oblique $\langle 111\rangle\{112\}$ slip system. Our output graphic files are too small in comparison with [18] to decide this question (arrival or emission of the dislocation). Nevertheless, it is well visible in fig. 5 that dislocation emission in the inclined slip systems $\langle 111\rangle\{101\}$ leads

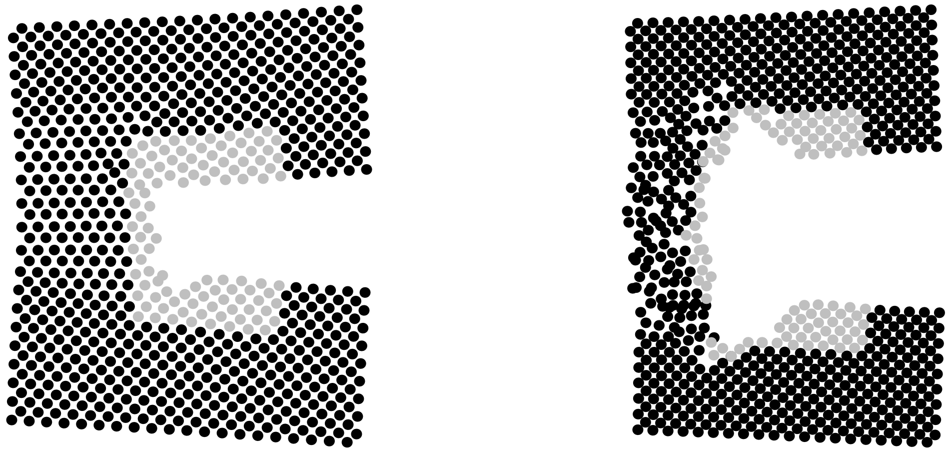

a) b)

Fig. 6. Detail from the atomic configuration at the Cu nano-inclusion at the left cavity corner in the middle of the crystal (layers 49–50) at time step a) $22\,400h$, b) $24\,500h$

to cavity blunting and its stability (fig. 5a), while an arrival or emission of dislocations from the oblique slip systems $\langle 111\rangle\{112\}$ (see fig. 2b) create a small jog in the crack front in fig. 5b. It was observed also in pure bcc iron in [18]. At time step 24 500 the structure in front of the cavity is more damaged after plastic deformation both from the $\{101\}$ and $\{112\}$ slip planes but the cavity is stable, similar to bcc iron.

3.4. Cu nano-inclusion along the crack front

In this case plastic deformation started again via dislocation emission on the inclined $\{101\}$ planes from the free sample surface about at time step 22 900, which corresponds to $\sigma_A = 3.206$ GPa. It is below the applied stress needed for dislocation emission in pure bcc iron. Before it, already time step 22 400 (fig. 6a) and $\sigma_A = 3.136$ GPa, the possibility of crack deflections is monitored in the middle of the crystal, probably after an attempt to emit dislocation. The situation at time step 24 500 (comparable with pure bcc iron) in the middle of the crystal is shown in fig. 6b where also slip patterns from the oblique slip systems $\langle 111\rangle\{112\}$ at the cavity corners and in front of the cavity are visible. The structure in front of the cavity is more damaged after plastic deformation than in pure bcc iron, but the cavity is still stable similar as in pure bcc iron. Crack deflections in at the corners (fig. 6b) and damage in copper are caused by the emission of dislocations from the oblique slip systems $\langle 111\rangle\{112\}$ after the jog formation mentioned above.

The all presented results show that dislocation emission is easier in the Fe–Cu system in comparison with pure bcc iron since the energy needed for dislocation emission in bcc copper is lower [14] than in bcc iron. However, the stability of the blunted cavities in Fe–Cu systems seems to be weaker in copper region than in pure bcc iron, which could be related to the metastable character of bcc copper, which is discussed in [1] and [14].

Presented results are in a qualitative agreement with the results in [14], where the interaction of Cu nano-particles with a narrow crack in iron crystals of different orientation was investigated.

As follows from MD simulations [8, 10, 14], hindering of dislocations by Cu nanoprecipitate can contribute to hardening and embrittlement in dilute Fe–Cu alloys which is in agreement with experiments presented e.g. in [8, 19]. Damage at the blunted cavities covered by copper atoms presented here causes re-distribution of stress concentration which may leads to nucleation of new cracks at the cavities and contribute also to copper embrittlement observed in fracture experiments [6] with irradiated ferritic older reactor steels.

4. Summary

Our MD simulations show that the initially blunted cavity $(001)[010]$ in pure bcc iron at temperature of 0 K is stable after dislocation emission in the inclined systems $\langle 111\rangle\{101\}$. Just a small crack deflection after the plastic deformation is observed in the middle of the crystal, well above Griffith level of loading. This ductile behavior is different from our previous 3D simulations [7, 14, 18] with the narrow cavity embedded in the crystal (of the same geometry and orientation) under the same loading conditions at 0 K, where brittle crack initiation was monitored. It indicates that the brittle→ductile transition can be recalled in bcc iron also at 0 K due to an initial crack blunting, which is theoretically possible also according to continuum predictions.

All the presented results show that the dislocation emission is easier in the Fe–Cu system in comparison with pure bcc iron since the energy needed for dislocation emission in bcc copper is lower than in bcc iron. Here, slip processes are observed both on the inclined $\{101\}$ planes and as well on the oblique $\{112\}$ planes, unlike pure bcc iron. However, stability of the blunted cavities in Fe–Cu systems seems to be weaker in copper region than in pure bcc iron, which could be related to metastable character of bcc copper. Presented results are in a qualitative agreement with our previous MD results, where interaction of Cu nano-particles with an atomically sharp crack $(-110)[110]$ in iron crystals of different orientation was investigated.

The results presented here may contribute to a better understanding of the mechanisms leading to copper embrittlement observed in fracture experiments with irradiated ferritic older reactor steels.

Acknowledgements

The work was supported by the Institute Research Plan AV0Z20760514 and by the grants GA CR No 101/07/0789 and GA AS CR KJB200760802. The access to the MetaCentrum clusters provided under the research intent MSM6383917201 is highly appreciated.

References

[1] Ackland, G. J., et al., Computer simulation of point defect properties in dilute Fe–Cu alloy using a many-body interatomic potential, Phil. Mag. A 75 (1997) 713–732.

[2] Beltz, G. E., Lipkin, D. M., Fisher, L. L., Role of crack blunting in ductile versus brittle response of crystalline materials, Phys. Rev. Letters 82 (1999) 4 468–4 471.

[3] Beltz, G. E., Machová, A., Reconciliation of continuum and atomistic models for the ductile versus brittle response of iron, Modelling Simul. Mater. Sci. Eng. 15 (2007) 65–83.

[4] Dienes, G. J., Paskin, A., Molecular dynamic simulations of crack propagation, J. Phys. Chem. Solids 48 (1987) 1 015–1 033.

[5] Fisher, L. L., Beltz, G. E., The effect of crack blunting on the competition between dislocation nucleation and cleavage, J. Mech. Phys. Solids 49 (2001) 635–654.

[6] Herztberg, R. W., Deformation and fracture mechanics of engineering materials, John Wiley & Sons, Second edition (1983) 405–410.

[7] Hora, P., Pelikán, V., Machová, A., Spielmannová, A., Prahl, J., Landa, M. and Červená, O., Crack induced slip processes in 3D, Engineering Fracture Mechanics 75 (2008) 3 612–3 623.

[8] Kizler, P., Koehler, C., Binkele, P., Willer, D., Al-Kssab, T., Ageing of steels by nucleation and growth of Cu precipitates understood by a synopsis of various experimental methods, molecular dynamics and Monte-Carlo simulations of energy minimization, Conference Proceedings, Third International Conference on Multiscale Materials Modeling, Freiburg, Germany, (2006) p. 736.

[9] Kočík, J., TEM microstructure after neutron irradiation (in Czech), Research Report MSM 267 224 4501(2005) Research center Řež (near Prague).

[10] Koehler, C., Kizler, P., Schmaudler, S., Atomistic simulations of precipitation hardening in α-iron: influence of precipitate shape and chemical composition, Modelling Simul. Mater. Sci. Eng. 11 (2005) 745–753.

[11] Lee, B. J., Wirth, B. D., Shim, J. H., Kwon, J., Kwon, S. C., Hong, J. H., Modified embedded-atom method interatomic potential for the Fe–Cu alloy system and cascade simulations on pure Fe and Fe–Cu alloys, Physical Review B 71 (2005) 184205-1-15.

[12] Machová, A., Ackland, G. J., Dynamic overshoot in α-iron by atomistic simulations, Modelling Simul. Mater. Sci. Eng. 6 (1998) 521–524.

[13] Machová, A., Residual stress in Fe–Cu alloys at 0 and 600 K, Computational Materials Science 24 (2002) 535–543.

[14] Machová, A., Spielmannová, A., Hora, P., 3D atomistic simulation of the interaction between a ductile crack and a Cu nanoprecipitate, Modelling Simul. Mater. Sci. Eng. 17 (2009) 035008 19 pp.

[15] Nagai, Y., Takadate, K., Tang, Z., Ohkubo, H., Sunaga, H., Takizawa, H., Hasegawa, M., Positron annihilation study of vacancy-solute complex evolution in Fe-based alloys, Physical Review B 67 (2003) 224202-6.

[16] Odette, G. R., On the dominant mechanism of irradiation embrittlement of reactor pressure vessel steels, Scripta Metall. 17 (1983) 1 183–1 188.

[17] Othen, P. J., Jenkins, M. L., Smith, G. D. W., Phythian, W. J., Transmission electron microscope investigations of the structure of copper precipitates in thermally-aged Fe–Cu and Fe–Cu–Ni, Philosophical Magazine Letters 64 (1991) 383–391.

[18] Pelikán, V., Hora, P., Machová, A., Spielmannová, A., Brittle-ductile behavior in 3D iron crystals, Czechoslovak Journal of Physics 55 (2005) 1 245–1 260.

[19] Phythian, W. J., Foreman, A. J., English, C. A., Buswell, J. T., Herington, M., Roberts, K., Pizzini, S., The structure and hardening mechanism of copper precipitation in thermally aged or irradiated Fe–Cu and Fe–Cu–Ni model alloys, Proc. 15th Int. Symp. On effects of radiation in Materials, Nashville, Tennessee, ASTM STP, 1990, also in AEA Technology Harwell Report AEA-TRS-2004.

[20] Rice, J. R., Limitation to the small scale yielding approximation for crack tip plasticity, J. Mech. Phys. Solids 22 (1974) 17–26.

[21] Savin, G. N., Stress Concentration Around Holes, New York: Pergamon Press, (1961).

[22] Spielmannová, A., Stress calculations at the crack front on atomistic level in 3D (in Czech), Research Study, ČVUT-FJFI-KMAT Prague (2004) 34 pp.